EEG-Based Learning System for Online Motion Sickness Level Estimation in a Dynamic Vehicle Environment

Chin-Teng Lin, *Fellow, IEEE*, Shu-Fang Tsai, and Li-Wei Ko, *Member, IEEE*

***Abstract*— Motion sickness is a common experience for many people. Several previous researches indicated that motion sickness has a negative effect on driving performance and sometimes leads to serious traffic accidents because of a decline in a person's ability to maintain self-control. This safety issue has motivated us to find a way to prevent vehicle accidents. Our target was to determine a set of valid motion sickness indicators that would predict the occurrence of a person's motion sickness as soon as possible. A successful method for the early detection of motion sickness will help us to construct a cognitive monitoring system. Such a monitoring system can alert people before they become sick and prevent them from being distracted by various motion sickness symptoms while driving or riding in a car. In our past researches, we investigated the physiological changes that occur during the transition of a passenger's cognitive state using electroencephalography (EEG) power spectrum analysis, and we found that the EEG power responses in the left and right motors, parietal, lateral occipital, and occipital midline brain areas were more highly correlated to subjective sickness levels than other brain areas. In this paper, we propose the use of a self-organizing neural fuzzy inference network (SONFIN) to estimate a driver's/passenger's sickness level based on EEG features that have been extracted online from five motion sickness-related brain areas, while either in real or virtual vehicle environments. The results show that our proposed learning system is capable of extracting a set of valid motion sickness indicators that originated from EEG dynamics, and through SONFIN, a neuro-fuzzy prediction model, we successfully translated the set of motion sickness indicators into motion sickness levels. The overall performance of this proposed EEG-based learning system can achieve an average prediction accuracy of ∼82%.**

***Index Terms*— Driving cognition, electroencephalography (EEG), learning system, motion sickness, online estimation.**

Manuscript received May 15, 2012; revised May 24, 2013; accepted July 14, 2013. Date of publication August 28, 2013; date of current version September 27, 2013. This work was supported in part by the UST-UCSD International Center of Excellence in Advanced Bio-engineering sponsored by the Taiwan National Science Council I-RiCE Program under Grant NSC-101-2911-I-009-101, the Aiming for the Top University Plan of National Chiao Tung University, the Ministry of Education of Taiwan under Contract 102W963, the Army Research Laboratory, and a cooperative under Grant W911NF-10-2-0022. *(Corresponding author: L.-W. Ko)*

C.-T. Lin and S.-F. Tsai are with the Institute of Computer Science and Engineering and Brain Research Center, National Chiao Tung University, Hsinchu 300, Taiwan (e-mail: ctlin@mail.nctu.edu.tw; judy.tsf@gmail.com).

L.-W. Ko is with the Department of Biological Science and Technology, Institute of Bioinformatics and Systems Biology, and Brain Research Center in National Chiao Tung University, Hsinchu 300, Taiwan (e-mail: lwko@mail.nctu.edu.tw).

Color versions of one or more of the figures in this paper are available online at http://ieeexplore.ieee.org.

Digital Object Identifier 10.1109/TNNLS.2013.2275003

I. Introduction

MOTION sickness is a common experience for many people, and it has received an increasing amount of attention; many researches have been performed on the subject. The symptoms of motion sickness are headache, sweating, disorientation, postural instability, dizziness, nausea, and vomiting. Reason and Brand [1] proposed that among the theories on the etiology of motion sickness, the most popular and accepted theory is the traditional sensory conflict theory. This theory states that when a pattern of inputs from the vestibular system, other proprioceptors, and the visual senses are not in accordance with stored patterns derived from recent transactions, the conflict could induce motion sickness. In previous human subject research, researchers attempted to identify those brain areas that are involved in these multimodal sensory system conflicts by means of clinical or anatomical methods. In previous clinical researches, the cortical activations during caloric [3] and galvanic vestibular [4] stimulations were studied using functional imaging technologies, such as positron emission tomography and functional magnetic resonance imaging. Among the available imaging technologies, electroencephalography (EEG) outperforms the other methods in terms of temporal resolution and portability. EEG studies that are related to motion sickness can be classified by the stimulus type, including vestibular stimuli [2], [36] and visual stimuli. Vestibular cues indicate that the body is stationary, whereas visual cues indicate that the body is moving. Vestibular stimuli have traditionally been provided using a rotating chair [5], [6], a parallel swing [7] or cross-coupled angular stimulation [8], to induce motion sickness in subjects. Previous researches indicated that the theta powers of the frontal and central brain areas are positively correlated with motion sickness that is induced by a parallel swing [7] and a rotating drum [5], [6]. Chelen *et al*. [8] reported increased delta- and theta-band power, but no significant change in the alpha-band power was observed when cross-coupled angular stimulation was employed to induce motion sickness. Visual stimuli can be provoked using an optokinetic drum that rotates around the yaw axis. Hu *et al*. [9] investigated motion sickness that is triggered by viewing an optokinetic rotating drum and found a higher net percentage increase in the EEG power in the 0.5–4-Hz band at electrode sites $C3$ and $C4$ than in the baseline spectra. From [10]–[13], the left/right motor, parietal, occipital, and occipital midline brain areas are motion sickness-related brain regions, and the correlation coefficients (CCs) in the alpha

bands of these regions exceed the CCs in other frequency bands. Furthermore, the EEG power responses in the occipital midline are more highly correlated with subjective sickness levels than the EEG power responses in other brain areas, which suggest that activation of the occipital midline could be useful for determining the stages of motion sickness. To collect training and testing data for our proposed learning system, we constructed a virtual reality (VR)-based dynamic driving simulator that provided both visual and vestibular stimuli to create motion sickness in a manner that is very similar to the stimuli induced by riding in a car. We implemented an EEG-based learning system to estimate people's motion sickness levels (MSLs) based on the real-time EEG power spectra from the left and right motors, parietal, occipital, and occipital midline brain regions, which are highly correlated with motion sickness. With EEG brain dynamics and self-reported MSLs from the driving simulators, the learning system obtains basic knowledge about each subject, such as the time lag between the EEG time series and the self-reported MSLs and the optimum number of eigenvectors to be used for performing principle component analysis (PCA). Then, the implemented estimation mechanism becomes functional whenever the driver or passenger's EEG dynamics becomes available. The prediction model used in our motion sickness estimation system is the self-organizing neural fuzzy inference network (SONFIN) [25]. There are several reasons to choose this neural-fuzzy network, although other choices of neural networks or fuzzy systems are also possible [32] ,[33], [35], [37]–[40]. First, the SONFIN is a hybrid system of neural networks and fuzzy logic. With a fuzzy-inference-type structured network, SONFIN can achieve higher learning accuracy than typical neural networks. Second, when compared with existing neural-fuzzy networks, SONFIN can perform both structure and parameter learning simultaneously, which enables it to construct itself dynamically online. Such an estimation system can be applied to detect a person's level of motion sickness early on, to prevent unexpected accidents because of motion sickness or to prevent motion sickness from occurring in people's daily lives.

The structure of this paper is outlined as follows. In Section II, we present the experimental setup, including the VR simulator, the experimental design, and the EEG data acquisition. Section III presents the architecture of the proposed MSL estimation system and the details of each function block. Section IV introduces three prediction models that are used in the estimation system. Section V discusses the experimental results that are obtained from the proposed system. Finally, Section VI contains some concluding remarks.

II. Experimental Setup

A. VR-Based Dynamic Driving Simulator

Unlike previous researches, we provided both visual and vestibular stimuli to the participants through a compelling VR environment that comprised a 360° projection of a VR scene and a motion platform with six degrees of freedom to induce the motion sickness (Fig. 1). With this setup, we expected to create motion sickness in a manner that was similar to the

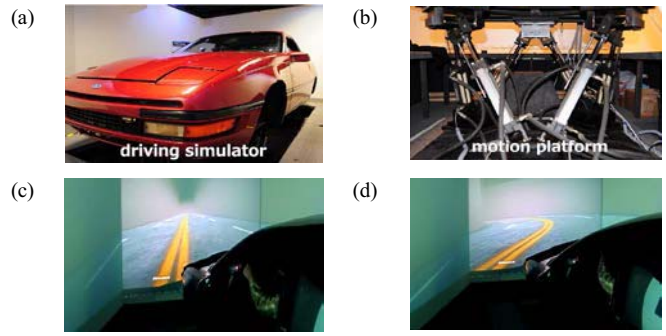

Fig. 1. VR environment comprises a motion platform and 360° projection of the VR scene. (a) Real car mounted on the motion platform. (b) Motion platform with six degrees of freedom to induce motion sickness. (c) VR scene that simulated driving through a tunnel with a straight road section. (d) VR scene that simulated driving through a tunnel with a winding road section.

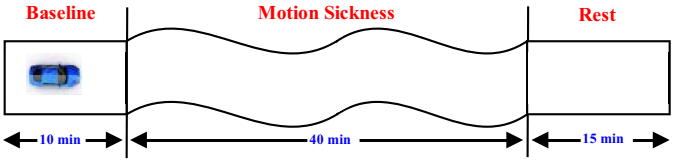

Fig. 2. Three-section motion sickness experimental protocol comprising a 10-min baseline section, to record the subject's baseline state, a 40-min winding road section, to induce motion sickness, and a 15-min rest section for recovery.

motion sickness that is experienced in our daily lives. During the experiment, the subjects were asked to sit inside an actual vehicle that was mounted on a motion platform, with their hands holding on to a joystick, which was able to continuously report their sickness level. VR scenes that simulate driving in a tunnel were programmed, to eliminate any possible visual distractions and to shorten the depth of the visual field, so the feeling of motion sickness could be easily induced. A three-section experimental protocol (Fig. 2) was designed to induce the motion sickness.

B. Experimental Design

A motion sickness experiment with a three-section protocol (Fig. 2) was designed. The first section was the baseline section, which comprised a 10-min straight road to record the subjects' baseline state. The second section was a 40-min motion sickness section, which comprised a long winding road and was presented to the subjects to induce motion sickness. Finally, a 15-min rest section on a straight road was displayed to allow the subjects to recover from their sickness. The subjects continuously reported their level of sickness using a joystick that had a continuous scale on its side. The results showed that such an experimental setting could successfully induce motion sickness in $>80\%$ of the subjects who participated in the research.

C. Subjects, EEG Data Acquisition, and Recording

Seventeen healthy right-handed volunteers with no history of gastrointestinal, cardiovascular or vestibular disorders or

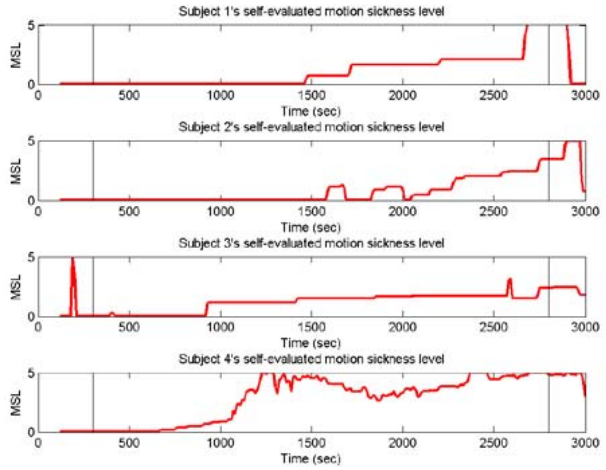

Fig. 3. Self-evaluated MSLs. From the four graphs, we observe that subject 2 felt motion sickness at ∼1500 s and that subject 4 felt motion sickness at ∼700 s. This information suggests that subject 4 could be more susceptible to motion sickness than subject 2. Because the MSL is self-evaluated by each subject, the variation in the MSL is meaningful, but the value of the MSL is, however, meaningless unless the MSL can be standardized.

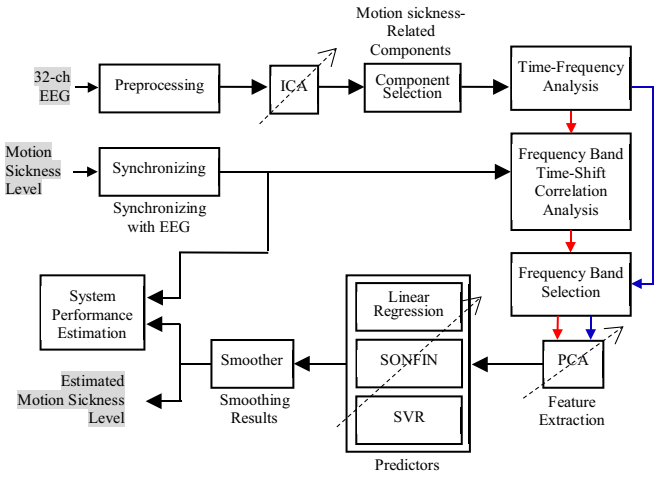

Fig. 4. Flowchart of the proposed learning system that estimates the MSL. Red lines: training data path. Blue lines: testing data path.

of drug or alcohol abuse, and who were taking no medication and had normal or corrected-to-normal vision participated in this experiment. A total of 33 sintered Ag/AgCl electroencephalography/electrooculography (EEG/EOG) electrodes with a unipolar reference at the right earlobe were used in the EEG data acquisition process. The EEG/EOG electrodes were placed according to a modified international 10–20 system and referenced to the right ear lobe. Before the data acquisition and recording were initiated, the contact impedance between the EEG electrodes and the cortex was calibrated to be >5 kΩ. The EEG data were then recorded with a 32-channel NuAmps (BioLink Ltd., Australia) and with 32-bit quantization at a sampling rate of 500 Hz. Simultaneously during the EEG recording, the level of motion sickness was continuously reported by each subject using a joystick with a scale that ranged from 0 to 65 535. The subjects were asked to raise or lower the scale to a higher or lower level whenever they felt more or less motion sickness, respectively, compared with their previous condition. In contrast to the traditional motion sickness questionnaire (MSQ), our mechanism allows the sickness level to be reported in real time without interrupting the experiment.

To ensure that each subject had the same maximum and minimum scales, we normalized each subject's level of motion sickness to a range from 0 to 5. The normalized self-reported MSLs are presented as a time series and are shown in Fig. 3.

III. Proposed MSL Estimation System

Fig. 4 presents a flowchart of the proposed learning system that was used to estimate the MSLs. The purpose of an MSL estimation system is to detect motion sickness in its early stages and to monitor the sickness level during an entire operation. The challenge in developing this system is to define a set of solid indicators, i.e., a feature set that, however, accurately interprets the MSLs. According to our previous researches, several brain regions are highly correlated with motion sickness; therefore, we designed several approaches to estimate the MSLs. One approach was to use a broadband EEG signal (1–30 Hz) to obtain the training and testing data. Another approach was to select specific frequency bands that are highly correlated with motion sickness. The use of PCA as a feature selector was an option for extracting the signals that had the largest variances. We adopted three types of prediction models: SONFIN as the primary prediction model, and support vector regression (SVR) and linear regression (LR) as the comparison models. The learning and estimation system concept was composed of eight functional units: an independent component analysis (ICA), component selection, a time–frequency analysis, a frequency band time-shifted correlation analysis, frequency band selection, feature extraction, a prediction model, and a smoother (with which the output curve of the estimated MSL was smoothed).

A. EEG Preprocessing

The raw EEG signals were first downsampled to 250 Hz and then filtered with a high-pass and low-pass filters. A high-pass filter with a cutoff frequency of 1 Hz and a transition bandwidth of 0.2 Hz was used to remove baseline-drifting artifacts, and a low-pass filter with a cutoff frequency of 50 Hz and a transition bandwidth of 7 Hz was used to remove muscular artifacts and line noise. Following these procedures, the preprocessed EEG signals were fed into the proposed estimation system for further analysis.

B. Independent Component Analysis

The EEG provides noninvasive measurements of the brain's electrical activity, which is recorded as changes in the potential differences between points on the human scalp. Because of the volume conduction through the cerebrospinal fluid, skull, and scalp, EEG data collected from any point on the scalp could include activity from multiple processes that occur within a large brain volume. This complexity has made it difficult to relate EEG measurements to the underlying brain processes or

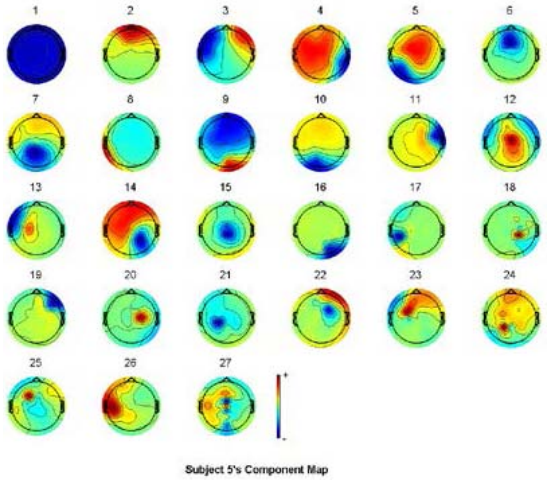

Fig. 5. Scalp topographies of subject 5. Components 2 and 3 represent eye blinks and eye rolling, respectively, whereas components 5, 7, 10, and 14 are the scalp topographies that are associated with the midline occipital, parietal, lateral occipital, and right motor brain regions, respectively.

to localize the sources of the EEG signals [14]. Furthermore, EEG recordings are usually contaminated by various artifacts, including eye blinks, muscle artifacts, and indoor power-line noise. Thus, the blind source separation (BSS) problem [15], [16] becomes an important issue in EEG-based researches. One popular method to solve the BSS problem is the application of ICA to identify the linear projections that maximize the mutual independences of the estimated components. Makeig *et al*. [17] also noted that ICA could be used to separate the problem of EEG [or magnetoencephalography (MEG)] source identification from the problem of source localization. This paper applied ICA to separate the observed multivariate EEG signals into independent components under the assumption of mutual statistical independence of non-Gaussian source signals.

The general representation of the ICA model can be simply denoted as $S = W^{-1}X$, where $S = [S_1, S_2, \ldots, S_n]^T$ represents the n independent sources, W^{-1} is the back-projection weighting matrix, and $X = [X_1, X_2, \ldots, X_n]^T$ is a vector of n observed signals. The purpose of the ICA algorithm is to define the back-projection weighting matrix W^{-1} and to create maximal statistical independency of the entire set of separated components, called S. Then, the motion sickness-related components [10] S_{cp}, where $S_{cp} = \left[S_{cp_1}, S_{cp_2}, \ldots, S_{cp_n}\right]^T$, were selected by the weighting distribution of the scalp topography, which was rendered by W^{-1} [18] as the region of interest for the power spectrum analysis and feature extraction. The scalp topographies shown in Fig. 5 are the components from subject 5.

C. Component Selection

After completing the ICA process, component clustering was analyzed using DIPFIT2 routines, a plug-in for EEGLAB, to determine the 3-D location of an equivalent dipole or dipoles based on a four-shell spherical head model. Among the components from all of the subjects, those subjects with similar scalp topographies, dipole locations, and power spectra were clustered. Five MSL-correlated component clusters that recruited 8–10 components from multiple subjects with similar topographic maps were regarded as robust component clusters. From the ICA results, we found that not all of the subjects presented every motion sickness-related component because the level of motion sickness induced by vestibular and visual stimuli exhibited significant individual differences. Based on the MSQ results and each subject's self-reported motion sickness, we were able to confirm which subjects did indeed feel motion sickness during the entire experimental session. Therefore, these extracted components were correlated with motion sickness. Next, we fed the ICA signals into the system and performed a time–frequency analysis. Based on our previous researches, we attempted to implement an EEG-based learning system to estimate the subjects' MSLs based on the EEG power spectra from the left and right motor, parietal, occipital, and occipital midline brain regions. The components of the five clusters are shown in Fig. 6.

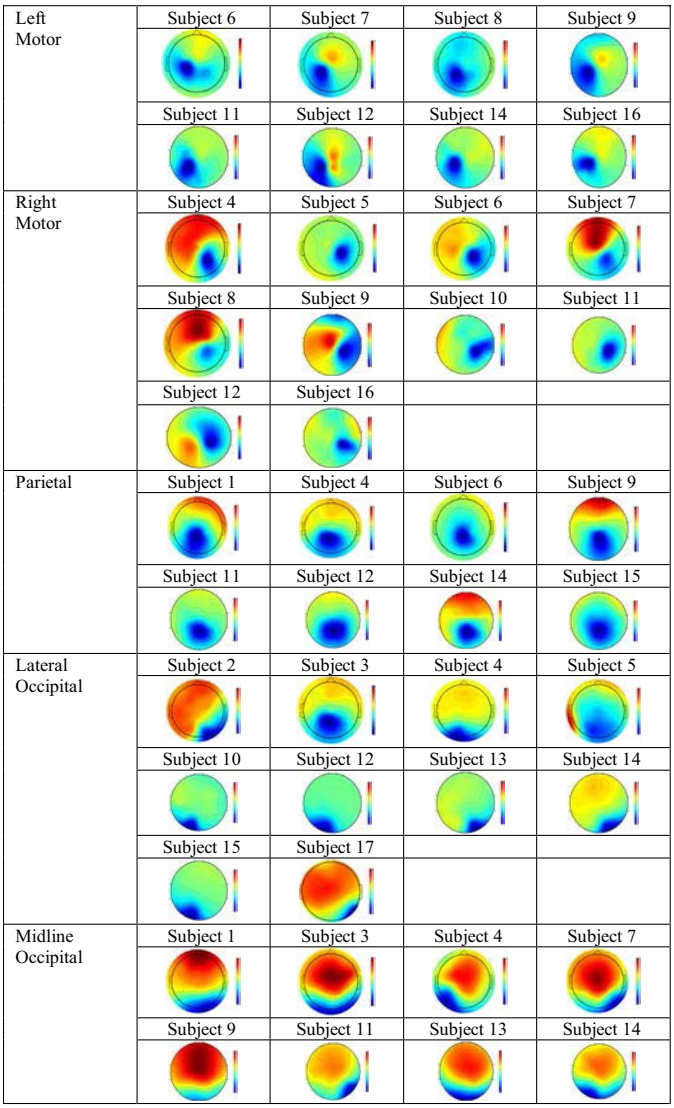

Fig. 6. Individual scalp topographies for five brain regions from 17 subjects. The left and right motor clusters are composed of 8 and 10 components, respectively; the parietal cluster comprises eight components, and the lateral and midline occipital clusters comprise 10 and 8 components, respectively.

D. Power Spectrum Analysis

A time–frequency analysis was performed to investigate the dynamics of the ICA power spectra. To provide a temporal resolution of 10 s, the spectra of the ICA activations were calculated using nonoverlapping windows of 10 s each. During this process, each window was further divided into several 250-point subwindows with 125-point overlaps. Then, each 250-point subwindow was zero-padded to 256 points to allow a fast Fourier transform with a frequency resolution of ∼1 Hz. The linear power spectrum density was then converted into a logarithmic scale (dB power). The resultant power spectrum time series of a single ICA component for each 60-min session comprised 50 frequency bins (from 1 to 50 Hz) with 10-s time interval steps.

E. Frequency Band Time-Frequency Analysis

During the training session, we attempted to determine the latency between the specific frequency band of the EEG dynamics and MSL by changing the time lag between them and then calculating the CCs. The time lag that was associated with the maximum CCs was used to synchronize the specific frequency bands of the EEG dynamics and the MSL (see Fig. 7. for the example).

F. Frequency Band Selection

In this step, specific frequency bands of the EEG dynamics were selected to perform feature extraction. These bands included broadband signals (1–30 Hz), the delta band (0.1–3 Hz), the theta band (4–7 Hz), the alpha band (8–12 Hz), the beta band (13–20 Hz), and the gamma band (21–30 Hz).

G. Feature Extraction

PCA [19], [20] was then used as an optional feature selector to summarize the variances and extract the first few principal components (PCs) of the specific frequency band of the EEG power spectrum time series for each selected motion sickness-related component after ICA. In this paper, the number of selected eigenvectors was determined during the PCA training process. Subject validation was performed to evaluate the estimation performance. Another approach to feature extraction comprised simply omitting PCA and selecting several specific frequency bands that were highly correlated with MSL in our previous and current researches. We will analyze the resulting performance later in this paper.

IV. MSL Prediction Models

In this paper, we propose the use of a SONFIN to estimate a driver's/passenger's MSL, and the system performance of SONFIN is compared with two benchmark systems, LR, and SVR.

The following section briefly describes the structure of each prediction model and introduces methods to estimate the performance of each predictor.

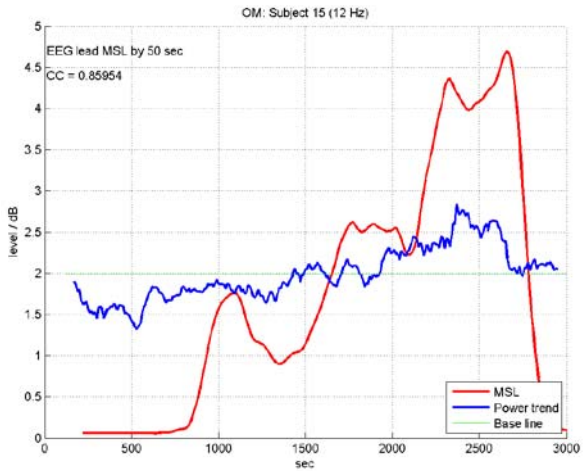

Fig. 7. Results of the time-shifted correlation analysis for the occipital midline brain area (OM) of subject 15. Considering the 12-Hz point of the EEG time series, the maximum CC was obtained when the EEG time series led the MSL by 50 s.

A. Linear Regression

Given a data set $\{y_i, x_{i1}, \ldots, x_{ip}\}_{i=1}^{n}$ of n statistical units, an LR model assumes that the relationship between the dependent variable y_i, and the p-vector of regressors x_i is linear. This relationship is modeled through a disturbance term or an error variable ε_i, which is an unobserved random variable that adds noise to the linear relationship between the dependent variables and the regressors. Thus, the model takes the following form:

$$y_i = \beta_1 x_{i1} + \cdots + \beta_p x_{ip} + \varepsilon_i = x_i^T \beta + \varepsilon_i \tag{1}$$

where β is a parameter vector whose elements are the regression coefficients and T denotes the transpose such that $x_i^T \beta$ is the inner product between vectors x_i and β. Variable y_i is estimated through minimization of the error expectation in (1).

B. Support Vector Regression

The support vector machine (SVM) is a popular approach for solving the problem of multidimensional function estimation and has been applied in various fields, such as classification and regression. When SVM is consistently employed for solving the problems of function approximation and regression estimation, it is denoted as SVR. SVR is a powerful technique for predictive data analysis [21], [22], with many applications in various areas of study. SVR is a complicated and heavily computational implementation of a prediction algorithm that is based on the use of structuring risk minimization principles to obtain good generalization capability [23], [24]. SVR is formulated as the estimation of a regression function $f(x_i, \omega)$ through the minimization of (2) as follows:

$$\min \frac{1}{2}\|\omega\|^2 + C\Sigma_i^n(\zeta_i + \zeta_i^*)$$
$$\text{subject to} \begin{cases} y_i - f(x_i, \omega) \leqq \varepsilon + \zeta_i^* \\ f(x_i, \omega) - y_i \leqq \varepsilon + \zeta_i \\ \zeta_i^*, \zeta_i \geqq 0, \quad i = 1, \ldots, n. \end{cases} \tag{2}$$

In this paper, a library of LIBSVM [24] was used for the SVR model construction with the radial basis function applied as its kernel function.

C. Self-Organizing Neural Fuzzy Inference Network

SONFIN [25] is composed of nodes, each of which has a finite fan-in of connections that are represented by weight values from other nodes and a fan-out of connections to other nodes. Associated with the fan-in of a node is an integration function f, which combines information, activation or evidence from other nodes. This function provides the net input for this node and is denoted as

$$\text{net\_input} = \mathrm{f}\left[\mathrm{u}_1^{(\mathrm{k})}, \mathrm{u}_2^{(\mathrm{k})}, \ldots, \mathrm{u}_\mathrm{p}^{(\mathrm{k})};\ \omega_1^{(\mathrm{k})}, \omega_2^{(\mathrm{k})}, \ldots, \omega_\mathrm{p}^{(\mathrm{k})}\right] \quad (3)$$

where $\mathrm{u}_1^{(\mathrm{k})}, \mathrm{u}_2^{(\mathrm{k})}, \ldots, \mathrm{u}_\mathrm{P}^{(\mathrm{k})}$ are inputs to this node and $\omega_1^{(\mathrm{k})}, \omega_2^{(\mathrm{k})}, \ldots, \omega_\mathrm{P}^{(\mathrm{k})}$ are the associated link weights. The superscript (k) indicates the layer number. The output for each node is an activation function value of its net input as follows:

$$\text{output} = \mathrm{o}_\mathrm{i}^{(\mathrm{k})} = \mathrm{a}(\text{net\_input}) = \mathrm{a}(\mathrm{f}) \quad (4)$$

where $\mathrm{a}(\cdot)$ denotes the activation function. The functions of the nodes in each of the five layers of the SONFIN structure are briefly described as follows.

Layer 1: Transmit inputs to the next node directly, without computation

$$\mathrm{f} = \mathrm{u}_\mathrm{i}^{(1)}, \quad \mathrm{a}^{(1)} = \mathrm{f}. \quad (5)$$

Layer 2: Calculate the output of Layer 1 into a fuzzy set

$$\mathrm{f}\left[\mathrm{u}_\mathrm{ij}^{(2)}\right] = -\frac{\left[\mathrm{u}_\mathrm{ij}^{(2)} - \mathrm{m}_\mathrm{ij}\right]^2}{\sigma_\mathrm{ij}^2}, \quad \mathrm{a}^{(2)} = \mathrm{e}^\mathrm{f}. \quad (6)$$

Layer 3: Perform a fuzzy rule with an AND operation

$$\mathrm{f}\left[\mathrm{u}_\mathrm{i}^{(3)}\right] = \Pi \mathrm{u}_\mathrm{i}^{(3)} = \mathrm{e}^{-[\mathrm{D_i}(\mathrm{x}-\mathrm{m_i})]^\mathrm{T}[\mathrm{D_i}(\mathrm{x}-\mathrm{m_i})]}, \quad \mathrm{a}^{(3)} = \mathrm{f}. \quad (7)$$

Layer 4: Normalize the firing strength calculated in Layer 3

$$\mathrm{f}[\mathrm{u}_\mathrm{i}^{(4)}] = \Sigma_\mathrm{i} \mathrm{u}_\mathrm{i}^{(4)}, \quad \mathrm{a}^{(4)}(\mathrm{f}) = \frac{\mathrm{u}_\mathrm{i}^{(4)}}{\mathrm{f}}. \quad (8)$$

Layer 5: Integrate all of the actions in Layer 5 to defuzzify the results. Each node in this layer corresponds to one output variable

$$\mathrm{f}[\mathrm{u}_\mathrm{i}^{(5)}] = \Sigma_\mathrm{i} \omega_\mathrm{i} \mathrm{u}_\mathrm{i}^{(5)}, \quad \mathrm{a}^{(5)}(\mathrm{f}) = \mathrm{f}. \quad (9)$$

D. Smoother

In our proposed system, the training and testing data sets were randomly selected from the EEG power spectrum time series and behavioral time series; therefore, there were time discontinuities in the estimated results. To suppress the fluctuation caused by the time discontinuity, a moving average was applied for smoothing the estimated output curve from SONFIN/LR/SVR.

For a given input vector X, where $\mathrm{X} = [\mathrm{X}_1, \mathrm{X}_2, \ldots, \mathrm{X}_\mathrm{n}]^\mathrm{T}$, the elements of the output vector Y of the moving average are given by

$$\begin{aligned}
\mathrm{Y_k} &= \mathrm{X_k}, && \mathrm{k} = 1, \mathrm{n} \\
\mathrm{Y_k} &= \frac{(\mathrm{X_{k-1}} + \mathrm{X_k} + \mathrm{X_{k+1}})}{3}, && \mathrm{k} = 2, \mathrm{n}-1 \\
\mathrm{Y_k} &= \frac{(\mathrm{X_{k-2}} + \mathrm{X_{k-1}} + \mathrm{X_k} + \mathrm{X_{k+1}} + \mathrm{X_{k+2}})}{5}, && \mathrm{k} = 3, \ldots, \mathrm{n}-2.
\end{aligned} \quad (10)$$

E. Performance Estimation

To estimate the performance of the different predictors, the Pearson product-moment correlation coefficient (PPMCC) and the root-mean-square error (RMSE) were applied.

In this paper, the PPMCC, denoted by CC, between the estimated and recorded MSLs, was obtained using (11)

$$\mathrm{cc} = \frac{\Sigma_{\mathrm{i}=1}^{\mathrm{n}}(\mathrm{MSL_i} - \overline{\mathrm{MSL}})(\mathrm{eMSL_i} - \overline{\mathrm{eMSL}})}{\sqrt{\Sigma_{\mathrm{i}=1}^{\mathrm{n}}(\mathrm{MSL_i} - \overline{\mathrm{MSL}})^2}\sqrt{\Sigma_{\mathrm{i}=1}^{\mathrm{n}}(\mathrm{eMSL_i} - \overline{\mathrm{eMSL}})^2}} \quad (11)$$

where n is the number of trials, and $\overline{\mathrm{MSL}}$ and $\overline{\mathrm{eMSL}}$ are the means of the recorded MSL and the estimated MSL, respectively. If the value of CC is high, then the two variables have a strong linear relationship, i.e., the higher the CC, the better the predictor [26].

The RMSE is another popular and useful index for assessing the performance of the predictors [26] and was calculated using the following equation:

$$\mathrm{RMSE} = \sqrt{\frac{\Sigma_{\mathrm{i}=1}^{\mathrm{n}}(\mathrm{MSL_i} - \mathrm{eMSL_i})^2}{\mathrm{n}}}. \quad (12)$$

A smaller RMSE represents better prediction by the proposed model.

V. Experimental Results and Discussion

A. Subject-Dependent Motion Sickness Prediction

In this paper, EEG data from 17 subjects were analyzed and applied to model the proposed learning system for MSL estimation. The CCs and the RMSEs were calculated to evaluate the performance of the system. For each subject, 70% of his or her EEG data and the corresponding behavior data (self-reported MSL) were used as a training data set, whereas the remaining 30% of the EEG and behavior data were collected as a testing data set. During each training procedure, the training data were randomly selected, and the same procedure was repeated 20 times to calculate the average CCs and RMSEs between the actual (self-reported) and estimated MSLs. Figs. 8–10 show the estimated MSLs of subject 6, subject 12, and subject 13, respectively. The results were estimated by EEG dynamics measured from different brain areas. For subject 6, the MSL curve estimated by the EEG dynamics measured from the left motor area has the highest correlation with the actual MSL curve; for subject 12, the MSL curve estimated by the EEG dynamics measured from the occipital midline brain area has the higher correlation with the actual MSL curve, whereas for subject 13, the MSL curve estimated by the EEG dynamics measured from the occipital midline brain area has the highest correlation with the actual MSL curve.

In our learning system, we propose the use of SONFIN as the prediction model for estimating a driver's/passenger's MSL, and the system performance of SONFIN is compared with two benchmark systems, including LR and SVR.

Table I compares the system performance of SONFIN, SVR, and LR when they are applied to the same broadband EEG power spectrum. The table lists the CCs between the actual and estimated MSL curves. The associated broken line graph

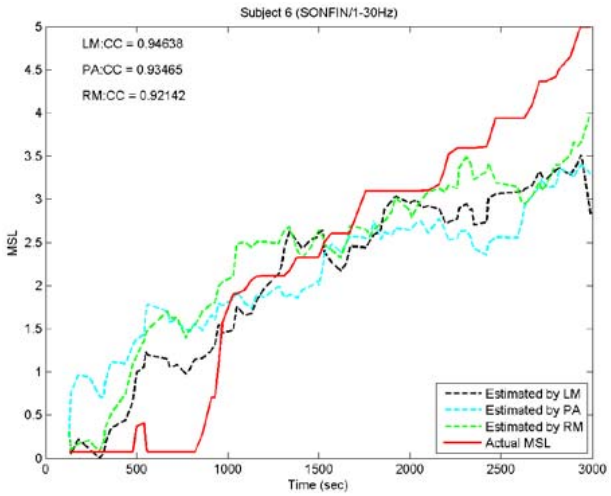

Fig. 8. Estimated MSL of subject 6. Black curve: estimated by the EEG dynamics measured from the left motor brain area (LM). Sky blue curve: estimated by the EEG dynamics measured from the parietal brain area (PA). Green curve: estimated by the EEG dynamics measured from the right motor brain area (RM).

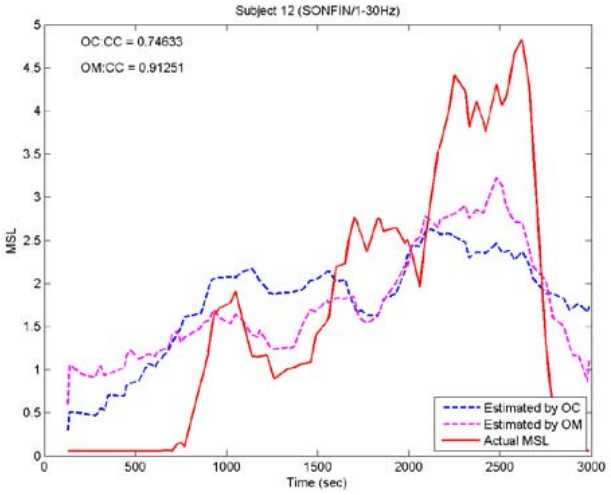

Fig. 9. Estimated MSL of subject 12. Navy blue curve: estimated by the EEG dynamics that were measured from the lateral occipital brain area (OC). Pink curve: estimated by the EEG dynamics that were measured from the occipital midline brain area (OM).

is shown in Fig. 11. From this graph, we see that SONFIN and SVR outperform LR when PCA is omitted, and SONFIN is slightly better than SVR in this situation.

Previous researches indicated that the delta, theta, and alpha powers of certain brain areas are positively correlated with motion sickness. In this paper, we apply our proposed learning system to various frequency bands of the EEG spectra, including the delta band (0.1–3 Hz), theta band (4–7 Hz), alpha band (8–12 Hz), beta band (13–20 Hz), and gamma band (21–30 Hz). The resulting CCs between the actual and estimated MSL curves are presented through a broken line graph and are shown in Fig. 12. From Fig. 12, we observe two facts. First, the gamma-band curve has a very similar trend as the broadband curve. Second, among all of the frequency bands, the alpha-band power has the highest CC in the occipital midline brain area (see Table III for the details). These two

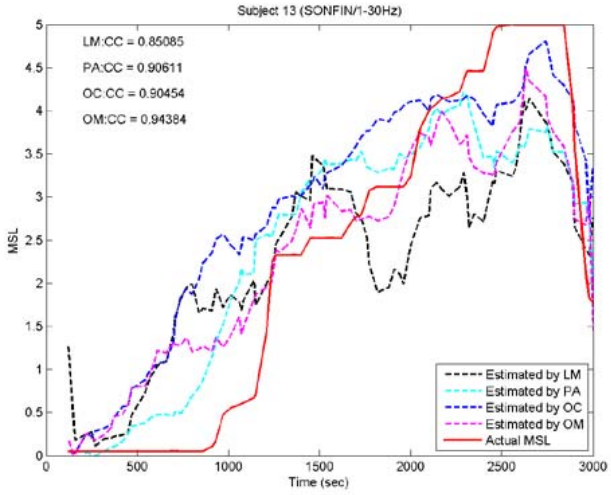

Fig. 10. Estimated MSL of subject 13. Black curve: estimated by the EEG dynamics that were measured from the left motor brain area (LM). Sky blue curve: estimated by the EEG dynamics that were measured from the parietal brain area (PA). Navy blue curve: estimated by the EEG dynamics that were measured from the lateral occipital brain area (OC). Pink curve: estimated by the EEG dynamics that were measured from the occipital midline brain area (OM).

TABLE I
FEATURE SELECTOR: NONE/FREQUENCY: BROADBAND

	SONFIN		SVR		LR	
	CC	RMSE	CC	RMSE	CC	RMSE
Left Motor	0.68 ± 0.04	1.30 ± 0.03	0.65 ± 0.03	1.36 ± 0.02	0.64 ± 0.03	1.32 ± 0.02
Parietal	0.68 ± 0.03	1.25 ± 0.03	0.66 ± 0.03	1.32 ± 0.02	0.65 ± 0.03	1.25 ± 0.02
Right Motor	0.67 ± 0.03	1.30 ± 0.02	0.68 ± 0.03	1.31 ± 0.02	0.60 ± 0.04	1.28 ± 0.02
Lateral Occipital	0.72 ± 0.03	1.20 ± 0.02	0.73 ± 0.02	1.22 ± 0.02	0.67 ± 0.04	1.24 ± 0.02
Occipital Midline	0.78 ± 0.03	1.17 ± 0.02	0.77 ± 0.03	1.18 ± 0.02	0.70 ± 0.04	1.26 ± 0.02

Broadband: 0.1-30 Hz

facts motivate us to combine frequency bands, such as the alpha and gamma bands or the alpha and beta bands. The results are very exciting. The orange curve in Fig. 13 shows the CCs between the actual MSL and MSL estimated by the combination of the alpha- and gamma-band EEG power spectra. The performance of the combination power spectrum is very close to the performance of the broadband power spectrum. Readers may refer to Tables II and IV for details.

Finally, we compare the performance of each prediction model when the input data are either the broadband or combination of the alpha- and gamma-band power spectra. Here, PCA is adopted as the feature selector, and the results are shown in Fig. 15. This broken line shows that the performance of SONFIN is better than that of SVR and LR. Furthermore, when the EEG dynamics are measured from the occipital midline brain area, each prediction model achieves its best performance. The significance can be examined by performing a multiple-comparison test. The inputs of the multiple-comparison test are the CCs between the actual and the estimated MSL curves that are estimated by each prediction model, whereas the input data of each prediction

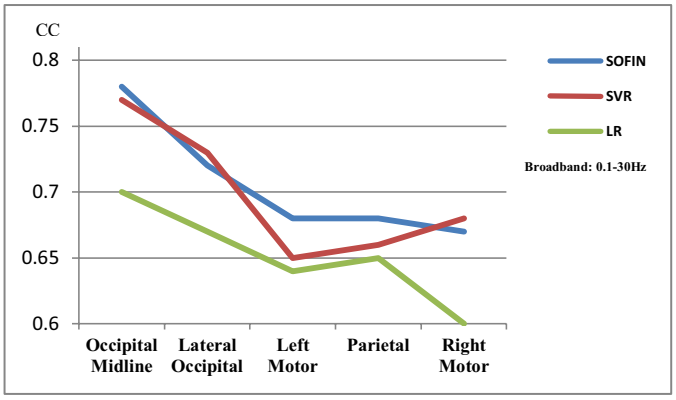

Fig. 11. Comparison of the performance between three prediction models when the input data are broadband EEG spectra (0.1–30 Hz). Vertical axis: CCs between the actual and estimated MSL curves. Horizontal axis: brain area from which the EEG dynamics were measured.

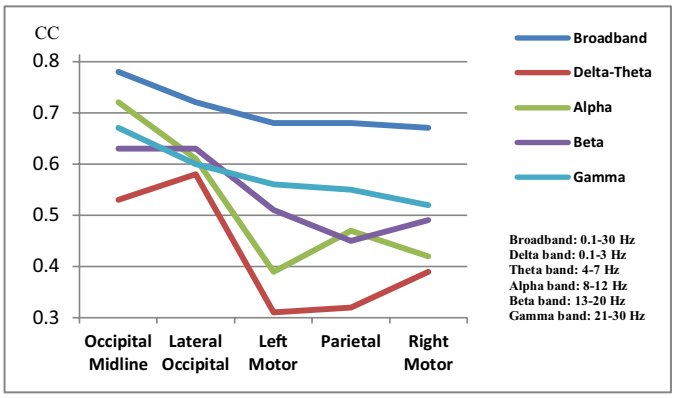

Fig. 12. CCs between the actual and estimated MSL curves when the different frequency bands of the EEG spectra are selected. In this scheme, SONFIN was selected as the prediction model. Vertical axis: CCs between the actual and the estimated MSL curves. Horizontal axis: brain area from which the EEG dynamics were measured.

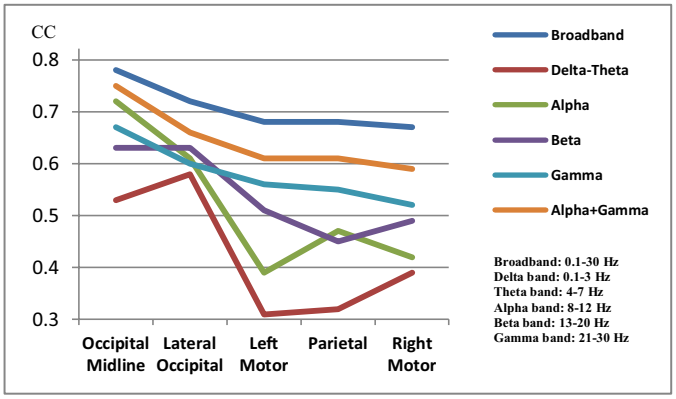

Fig. 13. CCs between the actual and estimated MSL curves when different frequency bands of the EEG spectra are selected. In this scheme, SONFIN was selected as the prediction model, but PCA was not used as an additional feature selector. Vertical axis: CCs between the actual and the estimated MSL curves. Horizontal axis: brain area from which the EEG dynamics were measured. Orange curve: performance of the combination of the alpha and gamma bands of the EEG spectra is second best when compared with that of the broadband EEG spectrum.

model are broadband EEG spectra that are measured from the occipital midline brain area. Fig. 16 shows that when PCA is omitted, the performance of SONFIN is better than

TABLE II
FEATURE SELECTOR: PCA/FREQUENCY: BROADBAND

	SONFIN		SVR		LR	
	CC	RMSE	CC	RMSE	CC	RMSE
Left Motor	0.72 ± 0.03	1.37 ± 0.06	0.69 ± 0.05	1.42 ± 0.02	0.72 ± 0.03	1.47 ± 0.02
Parietal	0.69 ± 0.05	1.30 ± 0.03	0.69 ± 0.05	1.42 ± 0.02	0.73 ± 0.04	1.48 ± 0.02
Right Motor	0.74 ± 0.04	1.30 ± 0.05	0.71 ± 0.03	1.38 ± 0.02	0.71 ± 0.03	1.44 ± 0.01
Lateral Occipital	0.80 ± 0.02	1.13 ± 0.03	0.75 ± 0.02	1.25 ± 0.02	0.77 ± 0.02	1.44 ± 0.01
Occipital Midline	0.82 ± 0.02	1.16 ± 0.03	0.79 ± 0.03	1.20 ± 0.03	0.80 ± 0.03	1.49 ± 0.01

Broadband: 0.1-30 Hz

TABLE III
FEATURE SELECTOR: PCA/FREQUENCY: ALPHA BAND

CC	SONFIN	SVR	LR
Left Motor	0.45 ± 0.07	0.47 ± 0.06	0.41 ± 0.09
Parietal	0.46 ± 0.04	0.55 ± 0.04	0.42 ± 0.06
Right Motor	0.50 ± 0.05	0.47 ± 0.06	0.48 ± 0.05
Lateral Occipital	0.65 ± 0.04	0.60 ± 0.03	0.64 ± 0.03
Occipital Midline	0.73 ± 0.03	0.74 ± 0.03	0.73 ± 0.03

Alpha band: 8-12 Hz

TABLE IV
FEATURE SELECTOR: PCA/FREQUENCY: ALPHA AND GAMMA BAND

CC	SONFIN	SVR	LR
Left Motor	0.65 ± 0.06	0.64 ± 0.05	0.65 ± 0.04
Parietal	0.66 ± 0.05	0.65 ± 0.05	0.64 ± 0.07
Right Motor	0.66 ± 0.04	0.61 ± 0.04	0.61 ± 0.04
Lateral Occipital	0.74 ± 0.03	0.71 ± 0.02	0.71 ± 0.03
Occipital Midline	0.79 ± 0.03	0.78 ± 0.03	0.78 ± 0.03

Alpha band: 8-12 Hz
Gamma band: 21-30 Hz

the performances of LR and SVR, but SONFIN significantly outperforms only LR. Furthermore, when PCA is present, only PCA + SONFIN significantly outperforms the performance from applying SONFIN alone. In other words, neither PCA + SVR NOR PCA + LR significantly outperforms SONFIN alone. That finding implies that SONFIN is more suitable for our proposed learning system compared with LR and SVR.

How does PCA improve the overall performance? Table VII compares the overall performance when PCA is present or absent when MSL is estimated by the broadband EEG spectrum. The results show that when PCA is present, the average CC will increase by 6.27%, 3.91%, and 12.61% when the prediction model is SONFIN, SVR, and LR, respectively.

B. Discussion

From Fig. 11, we see that SONFIN and SVR outperform LR when PCA is omitted, and SONFIN is slightly better than SVR in this situation. However, if PCA is adopted as the feature selector, the performance of SONFIN is better than

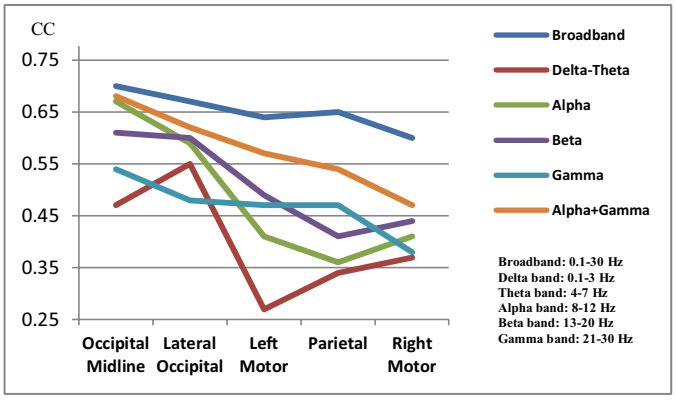

Fig. 14. CCs between the actual and estimated MSL curves when different frequency bands of EEG spectra are selected. In this scheme, LR was selected as the prediction model, but PCA was not used as the additional feature selector. Vertical axis: CCs between the actual and estimated MSL curves. Horizontal axis: brain area from which the EEG dynamics were measured. Orange curve: performance of the combination of the alpha and gamma bands of the EEG spectra is second best when compared with that of the broadband EEG spectrum.

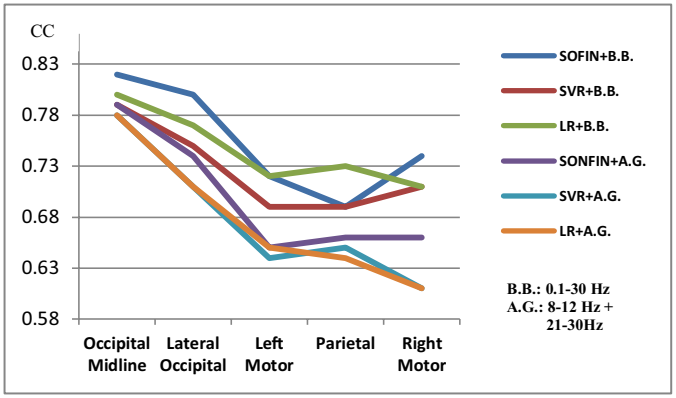

Fig. 15. Performance comparison between three prediction models when the input data are either the combination of the alpha and gamma bands of the EEG spectra (A.G.) or broadband EEG spectra (B.B.). In this comparison scheme, although the specific frequency band was selected, PCA was adopted as the feature selector. Vertical axis: CCs between the actual and the estimated MSL curves. Horizontal axis: brain area from which the EEG dynamics were measured. The results show that applying the SONFIN to the broadband EEG spectrum outperforms the performance of other combinations of the prediction model and input data.

that of SVR and LR, and the performance of LR is better than that of SVR. The results are shown in Fig. 15. Fig. 16 further suggests that, in our proposed learning system SONFIN, a neural-fuzzy network with online learning ability is a better choice for the MSL prediction model, when benchmarked against LR and SVR.

Figs. 11 and 15 also suggest that the broadband EEG power responses in the occipital midline brain area are more highly correlated with subjective sickness levels than the responses in other brain areas, irrespective of the prediction model that is used. Furthermore, the correlation analysis of all of the frequency bands shows that the delta- and theta-band powers are less correlated with subjective sickness levels than other frequency bands. Details are given in Figs. 13 and 14.

Table V shows that, although the alpha-band data account for only 16.7% of the broadband data, in the occipital midline brain area, the alpha-band power achieves up to 89% of the

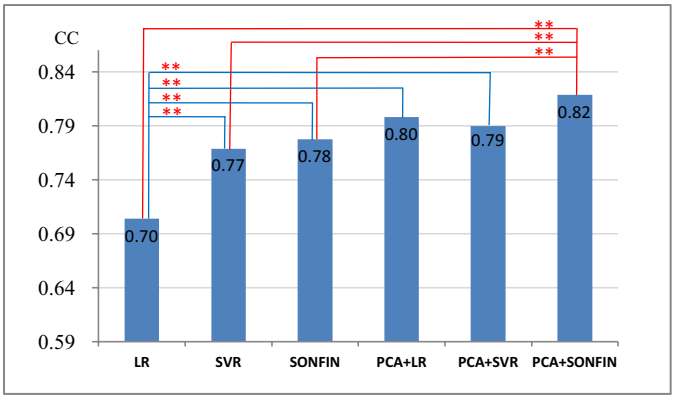

Fig. 16. Results of a multiple-comparison test between three prediction models, for which each model has PCA omitted or present. The inputs of the multiple-comparison test were the CCs between the actual and estimated MSL curves, whereas the input data of each prediction model were broadband EEG spectra that were measured from the occipital midline brain area. Horizontal axis: adopted prediction models. Vertical axis: values of the CCs. The results show that, when PCA is omitted, SONFIN outperforms the LR and SVR and significantly outperforms LR. Furthermore, when PCA is present, only PCA + SONFIN significantly outperforms the performance from applying SONFIN alone, whereas neither PCA + SVR NOR PCA + LR significantly outperforms SONFIN. (** significant, $\alpha = 0.05$).

TABLE V
FEATURE SELECTOR: PCA/FREQUENCY: BROADBAND, ALPHA BAND

$\frac{\text{CC of Alpha band}}{\text{CC of Broadband}}$ x 100%	SONFIN	SVR	LR
Left Motor	62.50%	68.12%	56.94%
Parietal	66.67%	79.71%	57.53%
Right Motor	67.57%	66.20%	67.61%
Lateral Occipital	81.25%	80.00%	83.12%
Occipital Midline	89.02%	93.67%	91.25%
Average	**73.40%**	**77.54%**	**71.29%**

Alpha band: 8-12 Hz
Broadband: 0.1-30 Hz

TABLE VI
FEATURE SELECTOR: PCA/FREQUENCY: BROADBAND, ALPHA AND GAMMA BAND

$\frac{\text{CC of Alpha and Gamma band}}{\text{CC of Broadband}}$ x100%	SONFIN	SVR	LR
Left Motor	90.28%	92.75%	90.28%
Parietal	95.65%	94.20%	87.67%
Right Motor	89.19%	85.92%	85.92%
Lateral Occipital	92.50%	94.67%	92.21%
Occipital Midline	96.34%	98.73%	97.50%
Average	**92.79%**	**93.25%**	**90.71%**

Alpha band: 8-12 Hz
Gamma band: 21-30 Hz
Broadband: 0.1-30 Hz

prediction performance of the broadband EEG spectrum if SONFIN is used and up to 93% of the prediction performance of the broadband EEG spectrum if SVR is used, based on the CC analysis. The average prediction performance of the alpha-band power in the five motion sickness-correlated brain areas achieves 73.4% of the prediction performance of the broadband EEG spectrum if SONFIN is used.

Table VI shows that, although the alpha- and gamma-band data account for only 50% of the broadband data, in

TABLE VII
FEATURE SELECTOR: PCA/FREQUENCY: BROADBAND

$\left(1-\frac{\text{CC when PCA is absent}}{\text{CC when PCA is present}}\right)$x100%	SONFIN	SVR	LR
Left Motor	5.56%	5.80%	11.11%
Parietal	1.45%	4.35%	10.96%
Right Motor	9.46%	4.23%	15.49%
Lateral Occipital	10.00%	2.67%	12.99%
Occipital Midline	4.88%	2.53%	12.50%
Average	**6.27%**	**3.91%**	**12.61%**

Alpha band: 8-12 Hz
Gamma band: 21-30 Hz
Broadband: 0.1-30 Hz

the occipital midline brain area, the alpha- and gamma-band power achieves up to 96.34% of the prediction performance of the broadband EEG spectrum if SONFIN is used. The average prediction performance of the alpha- and gamma-band power in the five highly motion sickness-correlated brain areas achieves up to 92.79% of the prediction performance of the broadband EEG spectrum.

Finally, we would like to examine the performance of PCA alone in our proposed estimation system. Table VII shows that when the feature extractor PCA is used, then the CCs between the estimated and actual MSLs increase by an average of 6.27%, 3.91%, and 12.61%, which correspond to the prediction models SONFIN, SVR, and LR, respectively. This finding means that an extra feature extractor is helpful for enhancing the system performance.

Because of the lack of a method for standardizing and quantifying each subject's motion sickness, we did not evaluate the system performance in terms of the RMSE; we evaluated the system by CCs because the trend of self-reported motion sickness is more meaningful in this situation. However, we still use RMSE to evaluate the performance of SONFIN in comparison with the other two benchmark prediction models.

VI. CONCLUSION

As biosensing technologies continue to progress in the upcoming decades, the ability to image brain activity will move away from traditional brain-computer interface (BCI) settings into everyday environments through novel augmented BCIs, which are BCIs that can be used by individuals for everyday use [27], [28]. With biosensing technologies and mobile wireless EEG technologies [29]–[31], we can design a cognitive monitoring system that can monitor people's brain activity and alert them before they feel sick. Such a monitoring system could prevent people from being distracted by various motion sickness symptoms while driving or riding in a car.

How the current MSL that a person perceives compares with that the person felt 10 min ago is not an easy question for a subject to answer. A subject can determine whether the MSL he feels at the current stage is however, more or less than the MSL he felt in the previous stage. Therefore, we designed a learning system to predict the trend in the MSL by first extracting the motion sickness indicators and then using those indictors to predict the MSL through a neural network. Our proposed learning system provides a useful and efficient way to train the motion sickness estimation system by collecting training data from a VR driving simulator. In such an environment, the induced motion sickness was fairly similar to the motion sickness that is induced by an actual car ride.

Although the input signal EEG dynamics are usually noise sensitive and easily influenced by artifacts because of the microvolt scale of the amplitude, we solved the noise problem by performing an ICA to remove artifacts, such as eye blinks, muscle, and power-line noise. After several iterations, excluding EEG contaminations, the independent components were separated, localized, and extracted. For online processing, among all of the ICA components, we selected highly motion sickness-related components for an additional time–frequency analysis based on the knowledge obtained from our previous researches. By doing so, it was considerably easier to extract the valid motion sickness indicators from the dynamic EEG activations.

Because of their nonstationary nature, EEG dynamics do not exhibit unique characteristics in the frequency domain [34]. Therefore, a short-time Fourier transform was used to extract time–frequency features. Furthermore, rapid fluctuations in self-reported motion sickness usually increase the difficulty in performing the estimation. To overcome the fluctuation problem, the moving average method was applied to smooth the MSL that was reported by each subject. Nonetheless, another moving average was applied after the application of the prediction model to suppress output fluctuations as well.

Finally, through CC analysis, we suggest that the broadband EEG power responses in the occipital midline brain area are more highly correlated with subjective sickness levels than the responses in other brain areas, irrespective of the prediction model used. Among the frequency bands, the alpha and gamma bands of the EEG power spectrum are the valid indicators of motion sickness. Through a multiple-comparison test, we can further suggest that SONFIN, a neuro-fuzzy system with online self-constructing capability and online learning ability, is a better scheme to predict MSL, compared with LR and SVR. The results also show that, with an efficient feature extractor, the system prediction accuracy can definitely be improved.

With the help of biosensing and low-cost wireless EEG technologies, designing an online estimation system with an efficient learning mechanism through the application of a neural network approach is promising. In this paper, the overall performance of our proposed EEG-based learning system can achieve an average prediction accuracy of $\sim$82%. Our future work can focus on how to enhance the system's performance by finding a method for extracting perfect motion sickness indicators from a neural network.

ACKNOWLEDGMENT

The authors would like to thank Dr. Y. C. Chen, Dr. C. L. Lin, and S. W. Chuang for their help in developing the motion sickness experimental paradigm, performing the experiments, and collecting the EEG data sets.

REFERENCES

[1] J. Reason and J. J. Brand, *Motion Sickness*. San Francisco, CA, USA: Academic, 1975.

[2] T. Brand, M. Dieterich, and A. Danek, "Vestibular cortex lesions affect the perception of verticality," *Ann. Neurol.*, vol. 35, no. 4, pp. 403–412, 1994.

[3] O. Fasold, M. von Brevern, M. Kuhberg, C. J. Ploner, A. Villringer, T. Lempert, and R. Wenzel, "Human vestibular cortex as identified with caloric stimulation in functional magnetic resonance imaging," *NeuroImage*, vol. 17, no. 3, pp. 1384–1393, 2002.

[4] E. Lobel, J. F. Kleine, D. L. Bihan, A. Leroy-Willig, and A. Berthoz, "Functional MRI of galvanic vestibular stimulation," *J. Neurophysiol.*, vol. 80, no. 5, pp. 2699–2709, 1998.

[5] C. D. Wood, J. J. Stewart, M. J. Wood, F. A. Struve, J. J. Straumanis, M. E. Mims, and G. Y. Patrick, "Habituation and motion sickness," *J. Clinical Pharmacol.*, vol. 34, no. 6, pp. 628–634, 1994.

[6] S. J. Wood, "Human otolith–ocular reflexes during off-vertical axis rotation: Effect of frequency on tilt–translation ambiguity and motion sickness," *Neurosci. Lett.*, vol. 323, no. 1, pp. 41–44, 2002.

[7] J. P. Wu, "EEG changes in man during motion-sickness induced by parallel swing," *Space Med. Med. Eng.*, vol. 5, no. 3, pp. 200–205, 1992.

[8] W. E. Chelen, M. Kabrisky, and S. K. Rogers, "Spectral analysis of the electroencephalographic response to motion sickness," *Aviation, Space, Environ. Med.*, vol. 64, no. 1, pp. 24–29, 1993.

[9] S. Hu, K. McChesney, K. A. Player, A. M. Bahl, J. B. Buchanan, and J. E. Scozzafava, "Systematic investigation of physiological correlates of motion sickness induced by viewing an optokinetic rotating drum," *Aviation, Space, Environ. Med.*, vol. 70, no. 8, pp. 759–765, 1999.

[10] C. T. Lin, S. W. Chuang, Y. C. Chen, L. W. Ko, S. F. Liang, and T. P. Jung, "EEG effects of motion sickness induced in a dynamic virtual reality environment," in *Proc. 29th Annu. Int. Conf. IEEE Eng. Med. Biol. Soc.*, Aug. 2007, pp. 3872–3875.

[11] Y. C. Chen, J. R. Duann, C. L. Lin, S. W. Chuang, T. P. Jung, and C. T. Lin, "Motion-sickness related brain areas and EEG power activates," in *Foundations of Augmented Cognition. Neuroergonomics and Operational Neuroscience* (Lecture Notes in Artificial Intelligence), vol. 5638, New York, NY, USA: Springer-Veerlag, 2009, pp. 348–354.

[12] Y. C. Chen, J. R. Duann, S. W. Chuang, C. L. Lin, L. W. Ko, T. P. Jung, and C. T. Lin, "Spatial and temporal EEG dynamics of motion sickness," *NeuroImage*, vol. 49, no. 3, pp. 2862–2870, 2010.

[13] C. S. Wei, S. W. Chuang, W. R. Wang, L. W. Ko, T. P. Jung, and C. T. Lin, "Development of a motion sickness evaluation system based on EEG spectrum analysis," in *Proc. IEEE Int. Symp. Circuits Syst.*, May 2011.

[14] Y. K. Alexander, A. F. Andrew, A. F. Alexander, V. B. Sergei, and S. D. Boris, "Nonstationary nature of the brain activity as revealed by EEG/MEG: Methodological, practical and conceptual challenges," *Signal Process.*, vol. 85, no. 11, pp. 2190–2212, 2005.

[15] T. W. Lee, *Independent Component Analysis: Theory and Applications*. Norwell, MA, USA: Kluwer, 1998.

[16] S. Javidi, D. P. Mandic, and A. Cichocki, "Complex blind source extraction from noisy mixtures using second-order statistics," *IEEE Trans. Circuits Syst. I, Reg. Papers*, vol. 57, no. 7, pp. 1404–1416, Jul. 2010.

[17] S. Makeig, A. J. Bell, T. P. Jung, and T. J. Sejnowski, "Independent component analysis of electroencephalographic data," in *Advances in Neural Information Processing Systems*, vol. 8. Cambridge, MA, USA: MIT Press, 1996, pp. 145–151.

[18] J. J. Onton, M. Westerfield, J. Townsend, and S. Makeig, "Imaging human EEG dynamics using independent component analysis," *Neurosci. Biobehavioral Rev.*, vol. 30, no. 6, pp. 808–822, 2006.

[19] I. T. Jolliffe, *Principal Component Analysis*, 2nd ed. New York, NY, USA: Springer-Verlag, 2002.

[20] J. Li and D. Tao, "Simple exponential family PCA," *IEEE Trans. Neural Netw. Learn. Syst.*, vol. 24, no. 3, pp. 485–497, Mar. 2013.

[21] V. Cherkassky and F. Mulier, *Learning from Data—Concepts, Theory and Methods*. New York, NY, USA: Wiley, 1998.

[22] V. N. Vapnik, *The Nature of Statistical Learning Theory*. New York, NY, USA: Springer-Verlag, 1995.

[23] U. Thissen, M. Pepers, B. UstUn, W. J. Melssen, and L. M. C. Buydens, "Comparing support vector machines to PLS for spectral regression applications," *Chemometrics Intell. Lab. Syst.*, vol. 73, no. 2, pp. 169–179, 2004.

[24] C. C. Chang and C. J. Lin. (2011). "LIBSVM: A library for support vector machines," *ACM Trans. Intell. Syst. Technol.* [Online]. 2, pp. 27:1–27:27. Available: http://www.csie.ntu.edu.tw/~cjlin/libsvm

[25] C. F. Juang and C. T. Lin, "An on-line self-constmcting neural fuzzy inference network and its application," *IEEE Trans. Fuzzy Syst.*, vol. 6, no. 1, pp. 12–32, Feb. 1998.

[26] W. Klimesch, "EEG alpha and theta oscillations reflect cognitive and memory performance: A review and analysis," *Brain Res. Rev.*, vol. 29, nos. 2–3, pp. 169–195, 1999.

[27] L. D. Liao, C. T. Lin, K. McDowell, A. E. Wickenden, K. Gramann, T. P. Jung, L. W. Ko, and J. Y. Chang, "Biosensor technologies for augmented brain–computer interfaces in the next decades," *Proc. IEEE*, vol. 100, no. 13, pp. 1553–1566, May 2012.

[28] C. T. Lin, L. D. Liao, Y. H. Liu, I. J. Wang, B. S. Lin, and J. Y. Chang, "Novel dry polymer foam electrodes for long-term EEG measurement," *IEEE Trans. Biomed. Eng.*, vol. 58, no. 5, pp. 1200–1207, May 2011.

[29] S. Debener, F. Minow, R. Emkes, K. Gandras, and M. de Vos, "How about taking a low-cost, small, and wireless EEG for a walk?" *Psychophysiology*, vol. 49, no. 11, pp. 1617–1621, Nov. 2012.

[30] C. T. Lin, L. W. Ko, J. C. Chiou, J. R. Duann, R. S. Huang, S. F. Liang, T. W. Chiu, and T. P. Jung, "Noninvasive neural prostheses using mobile and wireless EEG," *Proc. IEEE*, vol. 96, no. 7, pp. 1167–1183, Jul. 2008.

[31] C. T. Lin, C. J. Chang, B. S. Lin, S. H. Hung, Chao C. F. Chao, and I. J. Wang, "A real-time wireless brain–computer interface system for drowsiness detection, biomedical circuits and systems," *IEEE Trans. Biomed. Circuits Syst.*, vol. 4, no. 4, pp. 214–222, Aug. 2010.

[32] Y. Y. Lin, J. Y. Chang, and C. T. Lin, "Identification and prediction of dynamic systems using an interactively recurrent self-evolving fuzzy neural networ," *IEEE Trans. Neural Netw. Learn. Syst.*, vol. 24, no. 2, pp. 310–321, Feb. 2013.

[33] T. C. Silva, "Network-based high level data classification," *IEEE Trans. Neural Netw. Learn. Syst.*, vol. 23, no. 6, pp. 954–970, Jun. 2012.

[34] M. Arvaneh, C. Guan, K. K. Ang, and C. Quek, "Optimizing spatial filters by minimizing within-class dissimilarities in electroencephalogram-based brain-computer interface," *IEEE Trans. Neural Netw. Learn. Syst.*, vol. 24, no. 4, pp. 610–619, Apr. 2013.

[35] M. Shen, L. Lin, J. Chen, and C. Q. Chang, "A prediction approach for multichannel EEG signals modeling using local wavelet SVM," *IEEE Trans. Instrum. Meas.*, vol. 59, no. 5, pp. 1485–1492, May 2010.

[36] C. De Waele, P. M. Baudonnière, J. C. Lepecq, P. T. B. Huy, and P. P. Vidal, "Vestibular projections in the human cortex," *Experim. Brain Res.*, vol. 141, no. 4, pp. 541–551, 2001.

[37] A. Subasi, "Automatic recognition of alertness level from EEG by using neural network and wavelet coefficients," *Expert Syst. Appl.*, vol. 28, no. 4, pp. 701–711, May 2005.

[38] M. K. Kiymik, M. Akin, and A. Subasi, "Automatic recognition of alertness level by using wavelet transform and artificial neural network," *J. Neurosci. Methods*, vol. 139, no. 2, pp. 231–240, Oct. 2004.

[39] I. I. Guler and E. D. Ubeyli, "Multiclass support vector machines for EEG-signals classification," *IEEE Trans. Inf. Tech. Biomed.*, vol. 11, no. 2, pp. 117–126, Mar. 2007.

[40] B. C. Kuo and K. Y. Chang, "Feature extractions for small sample size classification problem," *IEEE Trans. Geosci. Remote Sens.*, vol. 45, no. 3, pp. 756–764, Mar. 2007.

[41] G. Breyer, "Safe distance between vehicles" in *Proc. Conf. Eur. Directors Roads*, Apr. 2010.

[42] Road Safety of Authority. *Stopping Distances for Cars*, Ballina, Australia [Online]. Available: http://www.rulesoftheroad.ie/rules-for-driving/speed-limits/speed-limits_stopping-distances-cars.html

Chin-Teng Lin (F'95) received the B.S. degree from National Chiao-Tung University (NCTU), Hsinchu, Taiwan, in 1986, and the master's and Ph.D. degrees in electrical engineering from Purdue University, West Lafayette, IN, USA, in 1989 and 1992, respectively.

He is currently the Provost and a Chair Professor of electrical and computer engineering and the Director of Brain Research Center, NCTU. He was elevated to be an IEEE Fellow for his contributions to biologically inspired information systems in 2005 and was elevated International Fuzzy Systems Association Fellow in 2013. He is the co-author of *Neural Fuzzy Systems* (Prentice-Hall) and the author of *Neural Fuzzy Control Systems with Structure and Parameter Learning* (World Scientific). He has published more than 187 journal papers (H-index: 45) in the areas of neural networks, fuzzy systems, multimedia hardware/software, and cognitive neuro-engineering, including over 88 IEEE journal papers.

Dr. Lin has been elected as the Editor-in-Chief of the IEEE TRANSACTIONS ON FUZZY SYSTEMS since 2011. He served on the Board of Governors at IEEE Circuits and Systems Society from 2005 to 2008, the IEEE Systems, Man, Cybernetics Society from 2003 to 2005, the IEEE Computational Intelligence Society from 2008 to 2010, and the Chair of IEEE Taipei Section from 2009 to 2010. He was the Distinguished Lecturer of the IEEE CAS Society from 2003 to 2005. He served as the Deputy Editor-in-Chief of the IEEE TRANSACTIONS ON CIRCUITS AND SYSTEMS-II from 2006 to 2008. He was the Program Chair of the IEEE International Conference on Systems, Man, and Cybernetics in 2005 and a General Chair of the 2011 IEEE International Conference on Fuzzy Systems.

Shu-Fang Tsai received the B.S. degree from National Chiao-Tung University (NCTU), Hsinchu, Taiwan, in 1990, and the M.S. degree from the University of Southern California, Los Angeles, CA, USA, in 1993. She is currently pursuing the Ph.D. degree with the Institute of Computer Science and Engineering, NCTU.

Her current research interests include machine learning and biomedical signal processing.

Li-Wei Ko (M'98) received the B.S. degree in mathematics from National Chung Cheng University, Chiayi, Taiwan, in 2001, the M.S. degree in educational measurement and statistics from National Taichung University, Taichung, Taiwan, in 2004, and the Ph.D. degree in electrical engineering from National Chiao-Tung University (NCTU), Hsinchu, Taiwan, in 2007.

He is currently an Assistant Professor with the Department of Biological Science and Technology, and Brain Research Center, NCTU. His current research interests include neural engineering and mobile wireless healthcare, including EEG signal processing and applying computational intelligence technologies to analyze neural physiological activities associated with human cognitive functions and develop the mobile and wireless brain machine interface in daily life applications.

Dr. Ko serves as an Associate Editor of the IEEE TRANSACTIONS ON NEURAL NETWORKS AND LEARNING SYSTEMS and the *Journal of Neuroscience and Neuroengineering*. He is invited to the Editor Board of ISRN Automotive Engineering in 2013. He is the Technical Committee Member of Neural Network Technical Committee and Fuzzy Systems Technical Committee in IEEE CIS. He chaired a task force on "Fuzzy Modeling in Brain Computer Interactions and Cognitive Systems" in FSTC.